Fluorescence microscopy with diffraction resolution barrier broken by stimulated emission

Thomas A. Klar, Stefan Jakobs, Marcus Dyba, Alexander Egner, and Stefan W. Hell†

Max-Planck-Institute for Biophysical Chemistry, High Resolution Optical Microscopy Group, 37070 Göttingen, Germany

Edited by Daniel S. Chemla, E. O. Lawrence Berkeley National Laboratory, Berkeley, CA, and approved May 12, 2000 (received for review March 10, 2000)

The diffraction barrier responsible for a finite focal spot size and limited resolution in far-field fluorescence microscopy has been fundamentally broken. This is accomplished by quenching excited organic molecules at the rim of the focal spot through stimulated emission. Along the optic axis, the spot size was reduced by up to 6 times beyond the diffraction barrier. The simultaneous 2-fold improvement in the radial direction rendered a nearly spherical fluorescence spot with a diameter of 90–110 nm. The spot volume of down to 0.67 attoliters is 18 times smaller than that of confocal microscopy, thus making our results also relevant to three-dimensional photochemistry and single molecule spectroscopy. Images of live cells reveal greater details.

It is generally assumed that the extent of the focal spot of a microscope is not reducible beyond the wavelength of light λ, because diffraction demands an extent of at least $\lambda/3$ in the lateral and λ in the axial direction. In consequence, for more than a century, focused light was abandoned whenever higher spatial definitions were required. The diffraction limit also stimulated the invention of electron, scanning probe, and near-field optical microscopy, but these techniques are largely surface-bound and not able to image the intact cellular interior. Therefore, far-field light microscopy, encompassing the conventional and confocal fluorescence microscope, remained the most widely applied microscopy in biological research (1); however, the limited spot size hinders the visualization of fine subcellular structures.

We now report the generation of fluorescence focal spots of substantially reduced extent and their application to three-dimensional imaging. For the first time, the axial and lateral resolution of a lens is found to be in the same range (90–110 nm). Confocal sectioning is improved up to 5-fold. The improvement is attained by quenching through stimulated emission the excited fluorophores at the rim of the excitation focal spot with a beam whose wavelength is in the red edge of the fluorophore emission spectrum. Stimulated emission forces excited molecules to an upper vibrational level of the ground state, whose ultrafast vibrational decay (2) prevents re-excitation by the same beam. As a result, fluorescence can be entirely stopped (3–6). "Engineering" of the fluorescence spot, or point-spread-function (PSF) by stimulated emission depletion, was predicted to improve the resolution in the transverse direction (3, 5), and initial experiments with nanocrystals indeed confirmed an improvement by a factor of 1.3 (6). However, this moderate improvement was achieved along a single direction only, and it remained unclear whether it would be effective in biological imaging.

Physical Principles and Setup

Our setup used two synchronized trains of laser pulses: a train of visible pulses was used for excitation and a near-infrared counterpart for stimulated emission depletion (STED). Each excitation pulse was immediately followed by a STED pulse. The pulses originally stemmed from a mode-locked Ti:Sapphire laser (Coherent, Santa Clara, CA) emitting at a repetition rate of $f = 76$ MHz in the near-infrared. The pulses entered an optic parametric oscillator (Angewandte Physik und Elektronik, Berlin) with an intracavity frequency doubler. This system partly converted the Ti:Sapphire pulses into visible ones. The pulse trains were temporally adjusted by an optical delay stage and coupled into the setup by dichroic mirrors (Fig. 1*a*).

The duration of the visible pulses was 0.2 ps to ensure temporally defined excitation of the fluorophore. The near-infrared STED pulses were stretched by a grating to $\tau = 40$ ps. This allowed us to extend STED over a time period much longer than the relaxation time ($\approx$0.2 ps) of the vibrational substate of the electronic ground state into which the molecule is quenched. This is important because it allows the quenched molecules to escape re-excitation by the same beam through vibrational relaxation. Because we elected to use dyes with fluorescence wavelengths λ_{fl} from 650 to 800 nm, we adjusted the excitation and stimulation wavelengths to $\lambda_{exc} \approx 560$ nm and $\lambda_{STED} \approx 765$ nm, respectively. The broad spectral range of the fluorescence (80–120 nm) and the comparatively sharp spectrum of the laser light ($<$7 nm) enabled fluorescence separation from the laser by suitable emission filters, as in any fluorescence microscope. The fluorescence was collected in the backpropagating mode as the stimulating light beam passed straight through the sample.

To start off from the smallest possible "classical" spot, we used a 1.4 numerical aperture oil immersion lens (Leica 100×, Planapo, Wetzlar, Germany), which is a standard objective lens featuring the highest available semiaperture angle (67.3°). Fig. 1*b* displays an axial section of the focal spatial distribution of the excitation light featuring a pronounced maximum with a radial and axial extent of 220 and 560 nm, respectively. It was measured by registering the back-scattered light of a 100-nm-diameter gold bead that was scanned with a piezo stage operating at 5-nm precision (Melles Griot, Cambridge, U.K.). Behaving as a bright, point-like object, the gold bead efficiently probed the intensity in the focus and hence the spatial distribution of excitation, which we aimed to reduce in size (Fig. 1*b*).

The reduction of the extent of the fluorescence spot required a focal intensity distribution of the STED-beam that was intense around the focal point, but dark within it. This modification was accomplished by the use of an optical phase plate consisting of a planar glass substrate with a 1-μm-thin layer of MgF_2, evaporated on a central circular area. By introducing a delay by $\lambda_{STED}/2$, this layer reverts the sign of the wave amplitude with respect to the remaining ring-shaped area. Because we chose half of the total amplitude in the entrance pupil to be phase-reverted, the focused wave front produced destructive interference at the focal point and rendered a central minimum, as shown in the measurement in Fig. 1*c*. Whereas the excitation PSF featured the usual three-dimensional (3D) pattern, the STED-beam-PSF featured high intensity above and below the focal plane. In the transverse

This paper was submitted directly (Track II) to the PNAS office.

Abbreviations: PSF, point-spread-function; STED, stimulated emission depletion; 3D, three-dimensional; FWHM, full-width-at-half-maximum.

†To whom reprint requests should be addressed. E-mail: shell@gwdg.de.

The publication costs of this article were defrayed in part by page charge payment. This article must therefore be hereby marked "*advertisement*" in accordance with 18 U.S.C. §1734 solely to indicate this fact.

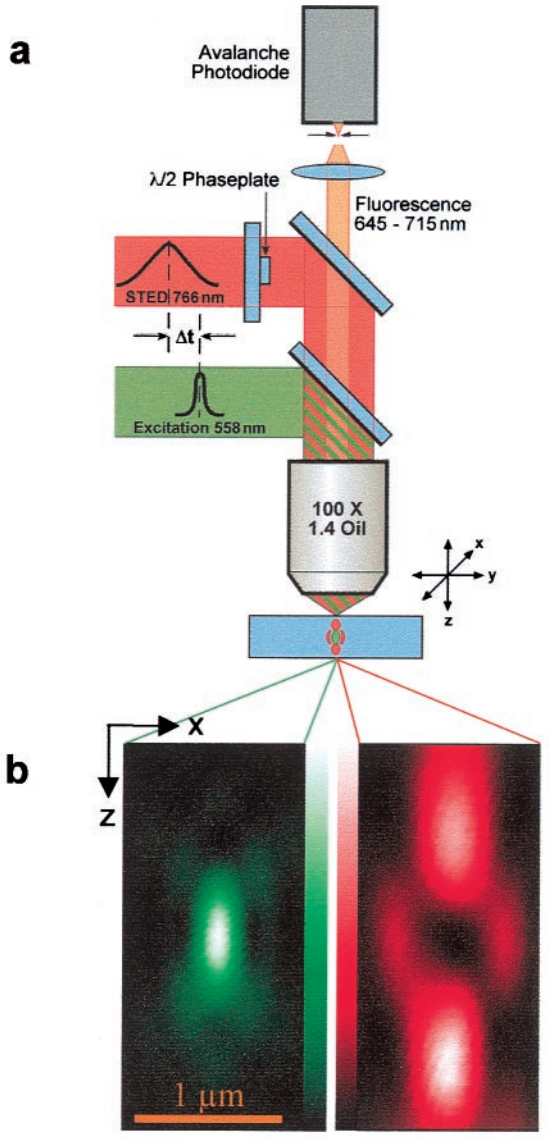

Fig. 1. Microscope. (*a*) Excitation pulses are followed by stimulated emission depletion pulses for fluorescence inhibition. After passing dichroic mirrors and emission filters, fluorescence is detected through a confocal pinhole by a counting photodiode. (*b*) Measured excitation PSF. (*c*) Measured STED-beam-PSF featuring local minimum at the center and intense maxima above and below the focal plane. Z denotes optic axis. The measurements of *b* and *c* are carried out with the pinhole removed.

direction, it also displayed a weak but non-negligible, doughnut-shaped first maximum that is expected to reduce the fluorescence spot also in the lateral direction.

Fig. 1 *b* and *c* indicates that the subtraction of the latter from the former should result in a narrower fluorescent spot. However, it is also apparent that the mere subtraction would increase the resolution only marginally, because the local minimum of the STED-beam-PSF is of about the same extent as the maximum of the excitation PSF. To really break the diffraction barrier, the minimum of the STED-beam-PSF must be narrower. This requirement is fulfilled by a nonlinear relationship between the intensity I_{STED} of the STED beam and the residual population of the fluorescent state, which is in fact theoretically expected (3, 5). If we denote the population of the fluorescent state with N_1 and that of the vibrational level of the ground state with N_0^*, the temporal change of the population is given by:

$$dN_1/dt = -N_1\sigma I_{\mathrm{STED}}/\hbar\omega + N_0^*\sigma I_{\mathrm{STED}}/\hbar\omega - N_1 k_{\mathrm{Fl}} \quad [1]$$

and

$$dN_0^*/dt = N_1\sigma I_{\mathrm{STED}}/\hbar\omega - N_0^*\sigma I_{\mathrm{STED}}/\hbar\omega - N_0^* k_{\mathrm{vib}}. \quad [2]$$

σ is the molecular cross-section for the transition and $\hbar\omega$ is the STED beam photon energy; k_{Fl} and k_{vib} are the rates for spontaneous emission and vibrational relaxation, respectively. The first and second term on the right hand side of Eq. **1** describe the stimulated emission from the fluorescent state and the re-excitation from the vibrational state by the stimulating beam, respectively. Whereas the third term on the right hand side of Eq. **1** describes the decay of N_1 by spontaneous emission, its counterpart in Eq. **2** describes the vibrational decay of N_0^*. If the focal intensity is low enough to render the rates of the stimulated transitions much slower than k_{vib}, re-excitation is negligible and $N_0^* \approx 0$. Hence, for a given duration τ of the STED pulse, the population of the fluorescent state and the remaining fluorescence obeys the proportionality $N_1 \propto e^{-\tau\sigma I_{\mathrm{STED}}/\hbar\omega}$ in good approximation. For higher intensities, the depletion of N_1 will be governed by the fast vibrational relaxation alone ($k_{\mathrm{vib}} \geq 3 \times 10^{12}$ s^{-1}). Altogether, this leads to a highly nonlinear relationship between N_1 and I_{STED}, the precise behavior of which is obtained by numerical computation (3, 5).

Results

This nonlinear relationship is indeed found in the experiment (Fig. 2*a*) in which we measure the fluorescence of the styryl dye LDS 751 (Molecular Probes) as a function of the STED-beam intensity for a given pulse length. The experiment was carried out by focusing without phaseplate onto a dye nanocrystal. The saturation of the depletion is so pronounced that, at STED-beam peak intensities $I_{\mathrm{STED}} \geq I_{\mathrm{STED}}^T \approx 0.75\ \mathrm{GW/cm^2}$, the fluorescence of the dye is suppressed to less than 10%. The "threshold intensity" I_{STED}^T is arbitrarily elected for orientation. We also note that the peak intensity was calculated as

$$I_{\mathrm{STED}}(z) \cong P_{\mathrm{STED}} \times S(z,0) / \left(2\pi f\tau \times \int_0^\infty S(z,r) r\, dr\right), \quad [3]$$

where $S(z, r)$ is the measured focal intensity distribution and r the radial coordinate. P_{STED} is the focused time-averaged power. The axial coordinate z is taken at the location of the maximum. Fig. 2*a* also allows us to predict the effect of the STED-beam-PSF of Fig. 1 when the focal intensities in the region of the maxima are $\geq I_{\mathrm{STED}}^T$: The fluorescence is inhibited in the whole focal region except for the innermost part of the spot. With increasing intensity, the area of inhibition grows and confines the fluorescence to an ever smaller volume. The result is a fluorescent spot with subdiffraction dimensions as the one shown in Fig. 2*d*.

The spot in Fig. 2*d* was probed by a 48-nm bead stained with the fluorophore LDS 751 with an intensity of $I_{\mathrm{STED}} \approx 2.8\ \mathrm{GW/cm^2}$, calculated as the average of the intensity of the two axial maxima. Because we placed a confocal pinhole in front of the detector, switching on and off the STED-beam automatically contrasted the narrowed focal spot with that of a confocal microscope (Fig. 2*b*). The difference in focal extent becomes obvious when comparing their XZ-sections shown in the inset. Because of the strong local maxima along the optic axis, the most pronounced difference is found in the axial direction. Whereas the confocal spot featured an axial full-width-at-half-maximum (FWHM) of 490 nm, that of the STED-fluorescence spot was only 97 nm.

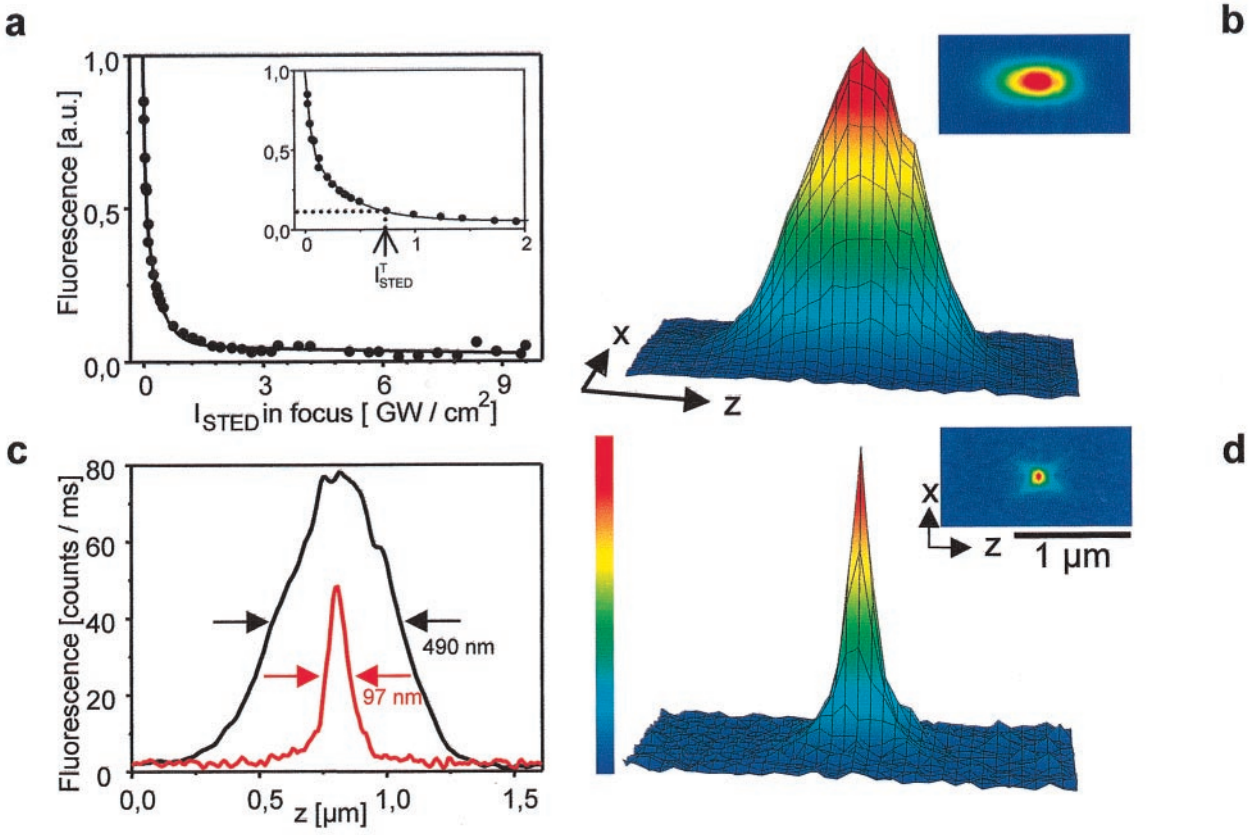

Fig. 2. (*a*) Fluorescence is a nonlinear function of stimulating intensity; 10% remaining fluorescence is obtained for I^{T}_{STED} corresponding to P_{STED} of 2.2 mW in the focus. (*b*) Surface plot of XZ-section (*Inset*) of confocal fluorescence spot for 1.4 oil immersion lens. (*d*) Same as *b* but with STED-beam PSF switched on. (*c*) Corresponding axial intensity profiles demonstrate 5.1-fold reduction of the axial width (FWHM) from 490 nm down to 97 nm.

We note that the STED-beam was switched on in the forward scan and off in the backward scan, line by line. Along with other spectroscopic evidence (6), this measure ruled out photobleaching as a potential cause of the observed spot size reduction. In the lateral direction, we measured a FWHM of 104 nm and 127 nm in x and y directions, respectively, meaning that the lateral resolution was doubled. The breaking of the resolution limit in the radial direction is a direct consequence of the doughnut-shaped first maximum of the STED-beam PSF. Because of the lower intensity in the ring, the lateral improvement was less pronounced than its axial counterpart. It could be enforced, however, by a differently optimized phase plate that should lead to a similar factor of spot size reduction also in the lateral direction.

Nevertheless, the nearly spherical spot size obtained with the present arrangement is particularly attractive because it reduces spot shape artifacts. Altogether, the 3D volume defined by the FWHM of the confocal spot was narrowed down by a factor of 18, so that we obtained a focal volume of 670 zeptoliter, which is for the first time below the 1 attoliter barrier. When compared with the FWHM volume of the main maximum of the conventional PSF in Fig. 1*b*, this reduction amounts to a factor of 28.

To compare the signal strength between the STED-fluorescence and the confocal spot, we display the non-normalized axial profiles in Fig. 2*c*, revealing a decrease of the peak height by 40% in the STED case. This decrease is comparatively low and is likely reduced by further optimization. Therefore the STED-beam indeed primarily suppresses the outer parts of the focus and leaves the center mostly unaffected.

The improved axial resolution is also evident in Fig. 3, in which we compare axial images of randomly dispersed 100-nm-diameter beads. The fluorescent beads were custom-labeled (Polysciences) with the dye Pyridine 2 (Lambdachrome, Göttingen, Germany). A

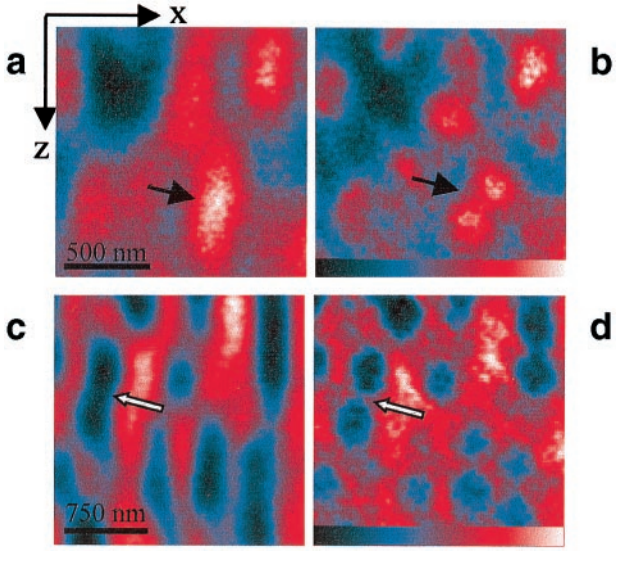

Fig. 3. XZ-images of 100-nm-diameter fluorescent beads (*a* and *b*) and of 100-nm-diameter negatively stained glass beads agglomerations (*c* and *d*) as observed in the confocal (*a* and *c*) and the STED-fluorescence (*b* and *d*) microscope. Note the artifacts indicated by arrows induced by the elongated spot in the confocal image and their reduction in the STED counterpart.

similar comparison is made for "negatively stained" beads: i.e., 100-nm unstained silica beads immersed in fluorescent solution. Negative staining was performed by dispersing 100-nm fused silica beads in Pyridine 2 dissolved in a Mowiol mounting medium [100 mM Tris·HCl, pH 8.5/9% Mowiol 4-88 (Hoechst)/25% glycerol]. In the regular confocal image (Fig. 3 *a* and *c*), the beads emerge as axially elongated entities. Importantly, this diffraction-induced misrepresentation is immanent to any focusing light microscope using a single lens. In the STED-fluorescence image (Fig. 3 *b* and *d*), however, the beads are largely spherical and better distinguished.

The peak intensities for efficient stimulated emission I_{STED} are higher than those required for 1-photon excitation because the rate of stimulation needs to be faster than the spontaneous emission. However, they are, by about two orders of magnitude, lower than the peak intensities of 200–500 GW/cm^2 successfully used in live cell multiphoton microscopy (7). This is attributable to the fact that the cross sections for 1-photon absorption and stimulated emission are similar. On the other hand, because of the longer pulse width, the pulse energies are of the same order. As potential optical limiting effects usually scale nonlinearly with the intensity (8–10), our method is live cell compatible.

Next we demonstrate that the STED method is indeed applicable to live cells. For this purpose, we labeled the vacuolar membrane of live yeast cells with the dye RH-414 (Molecular Probes). *Saccharomyces cerevisiae* strain RH 488 (*MAT**a**, his4, leu2, ura3, lys2, bar1-1*) were grown at 27°C in complete medium (1% yeast extract/2% peptone/2% glucose/20 mg/ml uracil and adenine) to an absorbance at 600 nm of approximately 0.8. The cell culture was diluted with one volume of 130 mM NaCl, 45 mM NaH_2PO_4, and 0.55 M sorbitol (pH 7.3). Vacuolar staining was accomplished by adding RH 414 to a final concentration of 70 μM from a 25 mg/ml EtOH stock solution. The uptake of RH 414 followed similar kinetics to the well characterized vital stain FM 4-64. Because the uptake of FM4-64 has been shown to be strictly time-, temperature-, and energy-dependent, we conclude that the labeled cells were alive (11). For microscopy analysis, the cells were embedded in 1% low melting agarose. Images were recorded 1 h after adding the dye. We also imaged live *Escherichia coli* bacteria labeled with the dye Pyridine 4 (Lambdachrome). For labeling the *E. coli* membranes, one volume of saturated ethanolic Pyridine 4 solution was diluted with 100 volumes of bacterial culture. Staining was performed for 1 h at room temperature. After a washing step, the cells were embedded in LB medium with 15 g/liter agar and were placed on a coverslip.

To reduce potential photostress, the yeast cells and the *E. coli* were imaged with calculated I_{STED} = 1.07 GW/cm^2 and 2.44 GW/cm^2, respectively. Because we focused into a watery medium, these intensities are present only at the interface between the glass coverslip and the watery medium. With increasing focusing depth, the intensities drop off as a result of spherical aberration induced by the concomitant refractive index mismatch. Although both intensities are greater than I^T_{STED} and therefore in the nonlinear range of the depletion curve of Fig. 2*a*, I_{STED} at the sample is expected to be significantly lower than in the case with the bead. Hence, we expect the resolution improvement by STED to be lower in the live cell sample.

Fig. 4 compares confocal axial images of the live yeast (*a*) and *E. coli* (*c*) cells with their STED-fluorescence counterparts in *b* and *d*, respectively. In Fig 4*a*, the axial images of the yeast vacuoles are observed as oval-shaped structures. Again, the diffraction-limited spot in the confocal microscope overemphasizes the vertical parts of the vacuolar membrane. In contrast, because of the axially narrowed focal spot, the STED-fluorescence image in Fig. 4*b* gives a more faithful picture of the spherical shape of the vacuoles of the live yeast cell (see arrow). In particular, they reveal the spherical shape of smaller vacuoles that cannot be recognized as such by the confocal microscope.

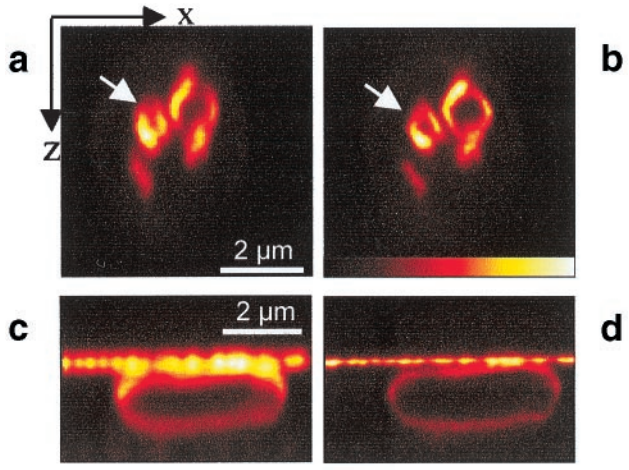

Fig. 4. Resolution improvement in live cells. XZ-images of a *S. cerevisiae* yeast cell with labeled vacuolar membranes with standard confocal resolution (*a*) and with axial resolution improved by STED (*b*). Whereas the confocal mode fails in resolving the membrane of small vacuoles, the STED microscopy better reveals their spherical structure. XZ-images of membrane-labeled *E. coli* show a 3-fold improvement of axial resolution by STED in *d* as compared with their simultaneously recorded confocal counterparts in *c*.

We noticed that after repeated imaging the dye dispersed in the cell, thus indicating that the STED beams induced photostress to the yeast cell. This was not observed when imaging the *E. coli*. In the STED-fluorescence *E. coli* image (Fig. 4*d*), the bacterial membrane is better outlined than in its confocal counterpart taken at the same time (*c*). To quantify the improvement of axial resolution in the sample, we precipitated a fine layer of fluorophore on the coverslip, which is easily noticed as a horizontal line in the images. We found that in the STED fluorescence image the axial resolution is improved by a factor of 3. We recorded several stacks of STED-images as the stained *E. coli* did not show notable alterations induced by imaging.

Of the dark red fluorescent dyes scrutinized, we found the following 17 compounds to display a fluorescence suppression of >90%: (*i*) styryls, such as Styryl 6, 7, and 8, LDS751, Pyridine 1 and 2, and RH 414; (*ii*) oxazines, such as Oxazine 170, Nile Red, and 7-AAD; (*iii*) carbocyanines such as DODCT, DTDCI, Cy 3, Cy 3.5, Cy 5, and (*iv*) the fluoresceines C-562 and C-563. (The dyes are tradenames of Lambdachrome, Amersham Pharmacia, or Molecular Probes. The fluorescence depletion was measured using uniform layers of saturated solutions in EtOH or DMSO mixed with Mowiol mounting medium in equal ratio. We note that the Stokes shift and cross-section may slightly vary with the solvent or mounting medium. The investigation of visible wavelength dyes for STED is a next step in our studies. We expect that a number of green, yellow, and red dyes will qualify for strong stimulated emission depletion.

Discussion and Outlook

We have demonstrated the breaking of the diffraction barrier in fluorescence light microscopy up to a factor of 2 in the lateral and 6 in the axial direction. The improvement of resolution along the optic axis was larger because the regions of strongest STED-beam intensity were located immediately above and below the focal plane. By positioning similarly intense beams in the lateral direction, a further substantial reduction of the fluorescent volume in this direction is anticipated.

In the STED-images of the live bakers yeast and *E. coli* cells, the gain in resolution is somewhat lower than what is found with the PSF measurement. This can be largely attributed to the fact that the cells were maintained in a watery environment whose

refractive index ($n = 1.34$) was significantly different from that of the glass coverslip ($n = 1.51$). Spherical aberration induced by the mismatch in refractive index reduces the local STED-beam intensity (12) and to a lesser extent the steepness of the STED-beam edges in the sample. This can be solved, however, by replacing the oil immersion lens with a water immersion lens and adapting the phase plate diameter to the water lens entrance pupil.

Besides the improvement of spatial resolution, STED also has other important applications. The instantaneous control of the fluorescence process under microscopy conditions opens up interesting perspectives in lifetime microscopy (4, 13) and nanospectroscopy from the nano- to the subpicosecond scale. STED should also open up new perspectives in the field of single molecule spectroscopy (14), such as the control of the excited state of individual molecules with tens of femtoseconds temporal resolution.

We will also address in the future whether repeated stimulated emission influences the photostability of the molecule. Whereas fast quenching to the ground state prevents intersystem crossing, the STED beam might also transiently excite the molecule into a higher singlet state. This would not have been directly observed in our experiment because the radiationless internal conversion is shorter by an order of magnitude than the duration of our STED pulse (40 ps). Putative transiently excited molecules would have also been quenched. STED pulses of several tens of picoseconds are preferred also because of the reduced probability of nonresonant multiphoton excitation from the ground state.

At much lower intensities and with a broader central minimum, the STED-beam could still be used as a "photophysical" 3D pinhole that, by surrounding the fluorescence spot, would relax the requirement of a tiny pinhole in confocal microscopy. Such a "soft" 3D pinhole could enable improved confocal imaging of deep regions of scattering specimens or eliminate focal aberrations of the excitation light. These applications should be facilitated by the fact that STED could be readily implemented in standard confocal beam scanners. STED can also be combined with total internal reflection microscopy to create spatially controlled excitation profiles (15).

The far-field lateral resolution demonstrated in Fig. 2 is equivalent to that obtained with most near-field optical microscopes; however, in the STED microscope, the resolution is entirely based on focused beams, does not imply delicate handling of a low-throughput scanning tip, and is able to image inside a 3D volume. Axial resolution can also be substantially improved by the coherent use of two opposing lenses, as is the case in 4Pi microscopy (16, 17). However, besides requiring external control of the phase of the counter propagating waves, this method also relies on subsequent data processing for interference effects removal. In contrast, the STED-concept is solely based on physical phenomena and can be synergistically combined with 4Pi microscopy to further improve the resolution (5). To the best of our knowledge, there is no reported alternative to the concept of STED that fundamentally improves the axial resolution in a single lens setting and without data processing. Computational image restoration can in addition improve the spatial resolution to a certain extent (18). The up to 2-times and 5- to 6-times larger optical bandwidth of our microscope, in radial and axial direction, respectively, and the fact that the central part of the fluorescence spot is not significantly suppressed are good preconditions to obtain a resolution by deconvolution of 40–50 nm in all directions, with a single lens.

The concept of STED-microscopy defeats the diffraction resolution barrier in a fundamental way. The demonstrated breaking of the diffraction barrier by a factor of 6 and the 18-fold reduction of the focal volume are not principle limits, because a further increase of the STED-intensity would decrease the focal volume even further. The precondition for further increasing the spatial resolution is to keep the STED-PSF at the center at zero level and to increase its intensity in the surrounding area. It is an important theoretical insight that, despite using diffraction limited beams, the concept of STED-fluorescence microscopy could reach far-field spatial resolution at the molecular scale.

In practice, however, the continuous increase in intensity will be challenged by concurrent photostress inflicted on the dye and the sample that may ultimately lead to increased bleaching and live cell incompatibility. At higher intensities and for some wavelengths, stimulated emission might be accompanied by molecular multiphoton excitation. It will be interesting to explore whether these challenges can be met by selecting fluorophores with higher stimulated emission cross-sections or other suitable conditions. Improving the capabilities of STED-fluorescence microscopy so to achieve resolution at the nanometer scale is a challenging but tempting scientific endeavor.

We also note that the depletion by stimulated emission is not restricted to fluorescence, but also applicable to nonfluorescent organic molecules with sufficient excited state lifetimes and significant stimulated emission cross-sections. In fact, our microscope demonstrates the control of the spatial and temporal distribution of molecules in their excited state. As the excited state is a first step in chemical transitions, our concept should enable restriction of chemical reactions, such as those occurring in photo induced three-dimensional data storage, to a spatial volume hitherto inconceivable with focused light.

We thank Dr. S. Schröder-Köhne for supplying us with the yeast strain RH 488 and W. Sauermann for manufacturing the phase plate. We acknowledge financial support by the Bundesministerium für Bildung, Wissenschaft, Forschung und Technologie (Bonn).

1. Pawley, J. (1995) *Handbook of Biological Confocal Microscopy* (Plenum, New York).
2. Birks, J. B. (1970) *Photophysics of Aromatic Molecules* (Wiley Interscience, London).
3. Hell, S. W. & Wichmann, J. (1994) *Opt. Lett.* **19,** 780–782.
4. Lakowicz, J. R., Gryczynski, I., Bogdanov, V. & Kusba, J. (1994) *J. Phys. Chem.* **98,** 334–342.
5. Hell, S. W. (1997) in *Topics in Fluorescence Spectroscopy*, ed. Lakowicz, J. R. (Plenum, New York), Vol. 5, pp. 361–422.
6. Klar, T. A. & Hell, S. W. (1999) *Opt. Lett.* **24,** 954–956.
7. Denk, W., Strickler, J. H. & Webb, W. W. (1990) *Science* **248,** 73–76.
8. Booth, M. & Hell, S. W. (1998) *J. Microsc. (Oxford)* **190,** 298–304.
9. König, K., Becker, T. W., Fischer, P., Riemann, I. & Halbhuber, K.-J. (1999) *Opt. Lett.* **24,** 113–115.
10. Koester, H. J., Baur, D., Uhl, R. & Hell, S. W. (1999) *Biophys. J.* **77,** 2226–2236.
11. Vida, T. A. & Emr, S. D. (1995) *J. Cell Biol.* **128,** 779–792.
12. Hell, S. W., Reiner, G., Cremer, C. & Stelzer, E. H. K. (1993) *J. Microsc.* **169,** 391–405.
13. Dong, C. Y., So, P. T. C., French, T. & Gratton, E. (1995) *Biophys. J.* **69,** 2234–2242.
14. Weiss, S. (1999) *Science* **283,** 1676–1683.
15. Cragg, G. E. & So, P. T. C. (2000) *Opt. Lett.* **25,** 46–48.
16. Hell, S. W., Schrader, M. & van der Voort, H. T. M. (1997) *J. Microsc. (Oxford)* **185,** 1–5.
17. Gustafsson, M. G. L., Agard, D. A. & Sedat, J. W. (1999) *J. Microsc. (Oxford)* **195,** 10–16.
18. Carrington, W. A., Lynch, R. M., Moore, E. D. W., Isenberg, G., Fogarty, K. E. & Fay, F. S. (1995) *Science* **268,** 1483–1487.